metals

MDPI

Article

Effect of Boron Content and Cooling Rate on the Microstructure and Boride Formation of β-Solidifying γ-TiAl TNM Alloy

Daniel Bernal [1,*], Xabier Chamorro [1], Iñaki Hurtado [1] and Iñaki Madariaga [2]

[1] Mechanical and Manufacturing Department, Mondragon University, Loramendi 4, 20500 Mondragon, Gipuzkoa, Spain; xchamorro@mondragon.edu (X.C.); ihurtado@mondragon.edu (I.H.)

[2] Materials and Processes Department, Industria de Turbopropulsores S.A.U, Parque Tecnológico No 300, 48170 Zamudio, Bizkaia, Spain; inaki.madariaga@itpaero.com

* Correspondence: dbernal@mondragon.edu; Tel.: +34-627-859-828

Received: 19 April 2020; Accepted: 23 May 2020; Published: 25 May 2020

Abstract: Boron is a unique and popular grain refiner element in cast titanium aluminide (TiAl) alloys, as it helps to improve mechanical properties if properly alloyed. However, the formation mechanism of different types of borides in cast TiAl alloys is not yet clearly understood. This study seeks to correlate the chemical composition and cooling rate during solidification of cast TiAl alloys, with the type of boride precipitated and the resulting microstructure. Several β-solidifying γ-TiAl alloys of the TNM family were cast, alloying boron to a starting Ti-44.5Al-4Nb-1Mo-0.1B (at.%) alloy. The alloys were manufactured with an induction skull melting furnace and poured into a stepped 2, 4, 8 and 16 mm thickness mold to achieve different cooling rates. On one hand, the results reveal that boron contents below 0.5 at.% and cooling rates during solidification above 10 K/s promote the formation of detrimental ribbon borides. On the other hand, boron contents above 0.5 at.% and cooling rates during solidification below 10 K/s promote the formation of a refined microstructure with blocky borides. Finally, the formation mechanisms of both ribbon and blocky borides are proposed.

Keywords: titanium aluminide; casting; boride; cooling rate; chemical composition

1. Introduction

Titanium aluminide (TiAl) alloys are promising lightweight materials because of their singular mechanical properties, such as high specific strength and good resistance against oxidation and corrosion. As a result, these materials are suitable for aircraft engines and gas-burning power-generation plants [1]. Of the available titanium aluminides, this work focuses on the β-solidifying γ-TiAl TNM (Ti-Nb-Mo) alloys, which are used in the low-pressure turbine blades of the new geared turbofan [2] to reduce fuel burn, pollutants, noise emissions and operating costs [3].

1.1. Solidification Pathway

Ti–Al–Nb–Mo (TNM) alloys solidify via the β-phase ($L \rightarrow L + \beta \rightarrow \beta \rightarrow \beta + \alpha \rightarrow \dots$), which leads to an isotropic structure, equiaxial grain, microstructure without texture and little micro-segregation. However, if there is a small variation in the chemical composition, peritectic solidification ($L \rightarrow L + \beta \rightarrow \alpha \rightarrow \dots$) can happen, leading to an anisotropic microstructure, segregation and texture [4]. Indeed, whenever a peritectic reaction happens, borides are no longer effective as grain refiners because the α-phase can nucleate on the β-phase dendrites invading the microstructure. In the case of the β-solidifying path, however, the Widmanstätten α-plates are precipitated from the β-phase with different orientation relationships to the parent phase, resulting in grain refinement [5].

There is a concentration limit that determines whether peritectic solidification will occur rather than β-solidification. This depends on the amount of aluminum and other alloying elements, which stabilize the α-phase with respect to β. Therefore, during the casting process, it must be ensured that no local displacement occurs towards the peritectic zone and the alloy solidifies entirely via β (Figure 1) [6].

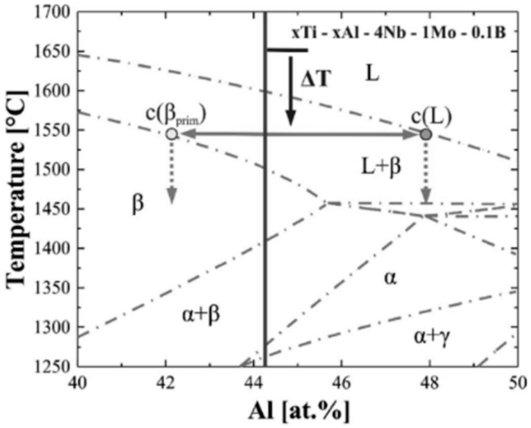

Figure 1. Detailed quasi-binary phase diagram of Ti–Al–Nb–Mo (TNM) alloys with varying aluminum concentrations. The discontinuous vertical lines represent the amount of aluminum in the β-phase and in the melt, respectively. Reproduced from [6] with the permission of Elsevier (2017).

1.2. Effect of Boron

Alloying with boron is a typical procedure to improve the mechanical properties of TNM alloys, as this refines the microstructure. However, the grain refinement mechanism associated with boron additions is not currently fully understood, and the two hypotheses proposed to date approach the phenomenon from different perspectives. First, state that grain refinement is achieved by primary nucleation of the β-phase on borides [7]. This is associated with boron contents above a critical value, which is compositionally dependent. For TNM alloys, this value is around 0.5 at.% of boron [8].

The second hypothesis relates to the grain refinement effect during the solid-state β to α-phase transformation: boron acts as an inoculant for the α-phase during decomposition of the β-phase [8,9]. This solid-state transformation is the most widely agreed-upon refinement mechanism, including in the present investigation. The nucleation of the α-phase from the β-phase is difficult due to the low coherency at the interfaces, so a large energy barrier needs to be overcome in order to nucleate an hexagonal close-packed (HCP) phase in a body centered cubic (BCC) matrix. As a result, only a few α-variants nucleate from the β-phase grain boundaries. Therefore, boron is added to form borides that act as inoculants to help the α-phase nucleate on their surface, which refines the microstructure of the alloy [10].

As stated by Yang et al., for a β-solidifying γ-TiAl with a boron content of 0.1 at.%, borides are thin and straight. Increasing the amount of boron to 0.3 at.% leads to curvy borides that are precipitated in inter-dendritic areas. An amount of 1 at.% of boron leads to coarse, long and straight borides precipitated from the liquid as well as borides formed in the β-phase that are precipitated in inter-dendritic areas. The results of their study indicated that the morphology of the borides is composition-dependent and that 0.5 at.% of boron is enough to refine the microstructure of the alloy given its low solubility in the β-phase [8].

The equilibrium Ti–Al–B–X phase diagram displays three intermediate compounds—TiB, Ti_3B_4 and TiB_2—with B27 and B_f, D7b and C32 crystal structures, respectively. Ribbon borides—TiB (B_f)—exhibit a preferential direction of growth and thus achieve a foil shape. The blocky borides—TiB (B27)—do not have a preferential direction of growth, but a mixture, so they achieve a thick, straight shape [9].

The two typical types of borides in TNM alloys are monoborides TiBs with B27 (blocky-type) and B_f (ribbon-type) crystal structures. These monoborides display metal-boron (MB) stoichiometry and

contain around 45 at.% of boron, with around 5–10 at.% of niobium and almost no aluminum [11,12]. However, they differ in the following ways [13]:

(1) Blocky borides (B27) provide nucleation points for the α-phase and are not detrimental to the elastic limit. In addition, they are beneficial for refining the microstructure. They are associated with slow cooling rates during solidification and no segregations;
(2) Ribbon borides (B_f) are detrimental because they do not help to nucleate the α-phase and reduce the elastic limit. This is due to the large β-boride interface, which may act as a crack initiation point. They are associated with high cooling rates during solidification.

Regarding the stability of the two types of borides present in TNM alloys, the blocky boride is stable, while the ribbon boride is metastable [14]. However, there is evidence that both types of borides are present in TNM alloys [7,8,10]. Thus, ribbon borides must be formed under non-equilibrium conditions, which are associated with fast cooling rates during solidification.

There is a lack of knowledge regarding the effect of cooling rate on the type of boride that is precipitated. Therefore, in this study, it is assumed that the cooling rate must be a key factor that promotes the formation of a certain type of boride given a fixed chemical composition, as the solubility of boron in the β-phase is limited and not yet clearly understood.

1.3. Research Goal

The present work seeks to correlate the effects of the amount of boron and cooling rate during solidification on the type of boride formed and the resulting microstructure for a castable TNM alloy. The aim is to establish the chemical composition and cooling rate that provides a microstructure without segregation and enough blocky borides to refine the microstructure. For this purpose, the base TNM alloy was alloyed with different amounts of TiB_2 and cast into a stepped 2, 4, 8 and 16 mm thicknesses aluminum mold.

2. Materials and Methods

2.1. Alloy Manufacturing and Melting Procedure

In this investigation, three TNM-based alloys were cast and studied in order to analyze the effect of the amount of boron and aluminum on the type of boride that is formed. Two new chemical compositions with 0.6 at.% and 1.5 at.% of boron were developed based on the TNM-0.1B master alloy. The TNM-0.1B master alloy was supplied by GfE and CP–Ti, CP–Al and TiB_2 were used as alloying elements.

The TNM-0.1B master alloy was melted within an induction skull melting (ISM) furnace in an argon atmosphere, a process that allows for melting of reactive alloys with almost no variation in chemical composition. CP–Ti and TiB_2 powder alloying elements were packed into CP–Al containers and added to the melt. Then, the molten metal was poured into a 2, 4, 8 and 16 mm thickness-stepped alumina molds preheated to 600 °C, in order to obtain different cooling rates and analyze their effects.

The stepped mold geometry was previously studied in a numerical simulation to analyze the cooling rate during solidification (Figure 2). FLOW-3D CAST® (v5.0, FLOW 3D, Santa Fe, NM, USA) was used to simulate the investment casting process with in situ TNM thermophysical properties for accurate numerical model development and results.

In order to empirically measure the cooling rate during solidification of highly reactive TiAl alloys, naked C-type thermocouples were employed for fast temperature readings. One thermocouple was placed in each step of the mold.

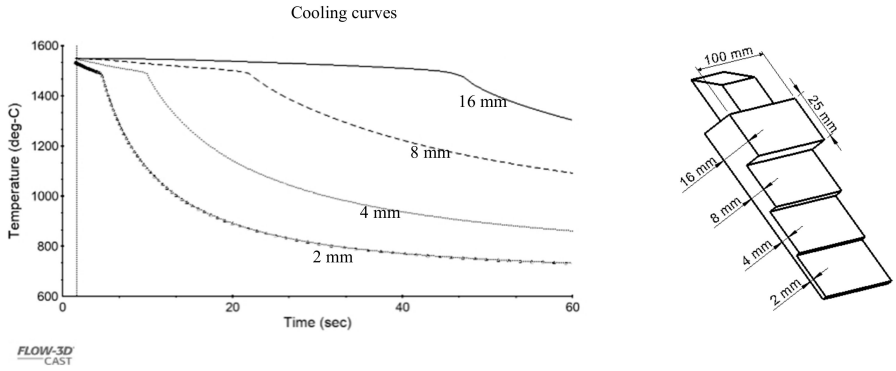

(**a**) (**b**)

Figure 2. (**a**) Computational simulation of a stepped specimen with 2, 4, 8 and 16 mm thicknesses; (**b**) sample of the stepped specimen with 2, 4, 8 and 16 mm thicknesses.

2.2. DSC and SEM Analysis

A differential scanning calorimeter (DSC) is a thermal analysis tool that is used to determine the temperature of phase transition and dissolution kinetics To determine the liquidus and solidus temperatures, a NETZSCH STA 449 F3 Jupiter DSC (NETZSCH, Selb, Deutschland) was employed. For the microstructure analysis and determination of semiquantitative local chemical composition, scanning electron microscopy (SEM) and energy-dispersive X-ray spectroscopy (EDS) were performed on a section of the polished samples with a Fei Nova Nanosem 450 (FEI Company, Hillsboro, OR, USA) in backscattered electrons (BSEs) and high-contrast mode.

3. Results

First, a preliminary analysis of the liquidus and solidus temperatures of the TNM-0.1B master alloy was performed with DSC at 10 K/min (Figure 3a), at temperatures of 1561 °C and 1503 °C, respectively. At a heating rate of 10 K/min (Figure 3b), the temperature at which dissolution of the α-phase occurred was about 1371 °C, and the temperature of the dissolution of the γ-phase was 1237 °C.

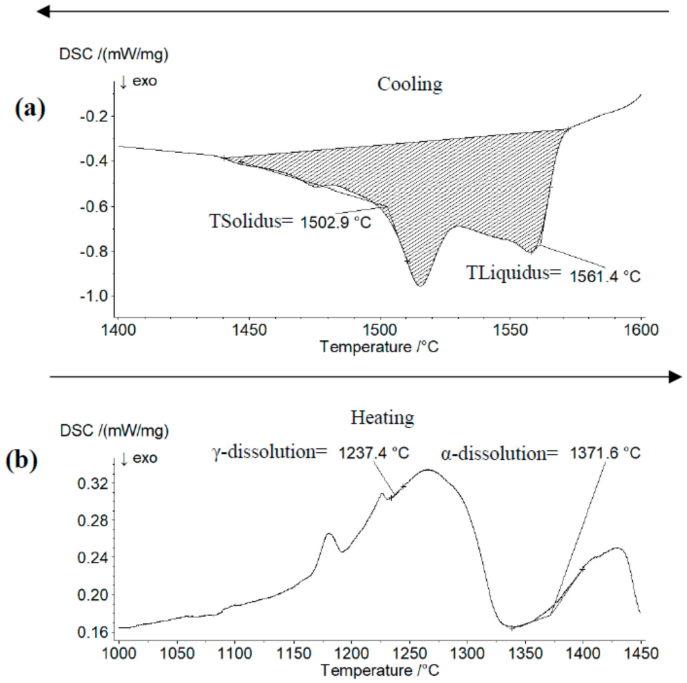

Figure 3. Differential scanning calorimeter (DSC) of base TNM-0.1B alloy: (**a**) solidification and, (**b**) phase dissolution.

3.1. Effect of Chemical Composition

Table 1 displays the real chemical compositions of the studied alloys.

Table 1. Real chemical compositions of the alloys obtained by inductively coupled plasma (ICP).

Concentration (at.%)	Ti	Al	Nb	Mo	B
TNM-0.1B (master alloy)	50.4	44.5	4	1	0.1
TNM-0.6B	50.1	44.6	3.6	0.9	0.6
TNM-1.5B	51.4	42.5	3.5	0.9	1.5

To highlight the effect of the chemical composition of each sample, the quickly cooled 2 mm, and the slowly cooled 16 mm steps were analyzed and compared.

3.1.1. Surface of the 2 mm Step (Fast Cooling)

The TNM-0.1B master alloy was the alloy with the lowest boron content. It exhibited different types and amounts of borides in different locations. While no segregations were observed on the surface, plenty of entangled ribbon borides and segregations were detected microns below the surface (Figure 4a), which are detrimental to the mechanical properties of the alloy. Figure 4b shows the region for which semi-quantitative chemical composition analysis of the different phases was performed (Table 2).

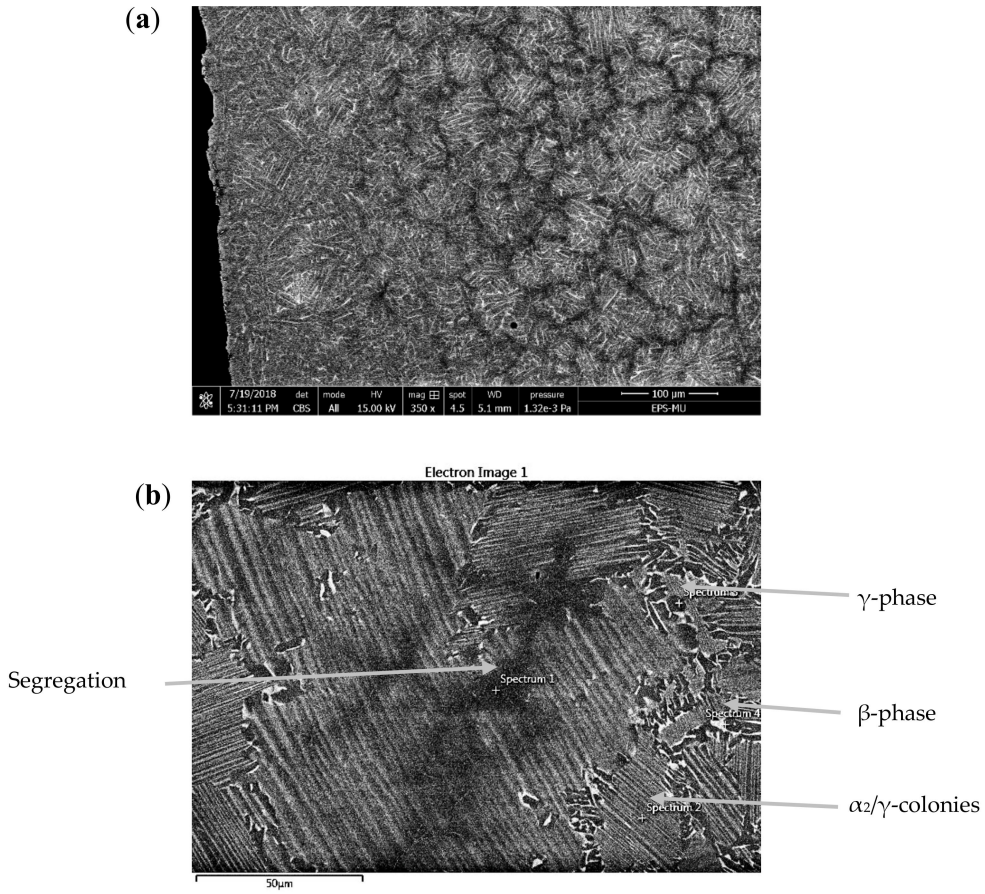

Figure 4. Backscattered electrons (BSE) image of the 2-mm step of the TNM-0.1B alloy: (**a**) ribbon borides inside segregations close to the surface and (**b**) energy-dispersive X-ray spectroscopy (EDS) of segregations (shown in black) with ribbon borides inside.

Table 2. Semi-quantitative chemical compositions of different phases and the region.

Chemical Composition, at.% Spectrum		Ti	Al	Nb	Mo
Phases	α_2/γ-colonies	51.7	43.3	4.2	0.9
	γ-phase	50.3	45.0	4.1	0.6
	β-phase	55.8	36.2	5.2	2.8
Region	Segregation	49.6	47.1	2.8	0.5

The microstructure was not homogeneous, and as a result, there were many segregations with entangled ribbon borides. The black regions were enriched with aluminum and depleted with β-stabilizing elements (niobium, molybdenum). The lamellar microstructure displayed a chemical composition similar to that of the bulk alloy, while the γ-phase was slightly enriched with aluminum and the β-phase enriched with the β-stabilizing elements, especially in molybdenum, which is a stronger β-stabilizing element than niobium.

In the modified TNM-0.6B, randomly dispersed segregations with ribbon borides inside were clearly observed, but there were not as many as in TNM-0.1B (Figure 5). Some blocky borides were detected.

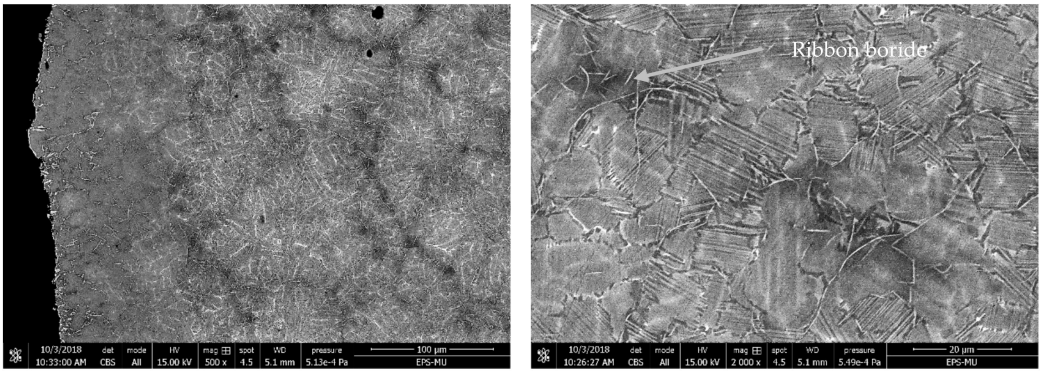

(**a**) (**b**)

Figure 5. BSE image of the 2 mm step of the modified TNM-0.6B alloy: (**a**) ribbon borides inside segregations close to the surface and (**b**) detailed image of the ribbon borides.

The modified TNM-1.5B alloy displayed (Figure 6) a more homogeneous microstructure than the modified TNM-0.6B alloy, as there were few randomly dispersed segregations with ribbon borides close to the surface. A higher amount of β-phase was observed, apparently as a result of a reduction in aluminum within the bulk chemical composition. Some blocky borides were observed.

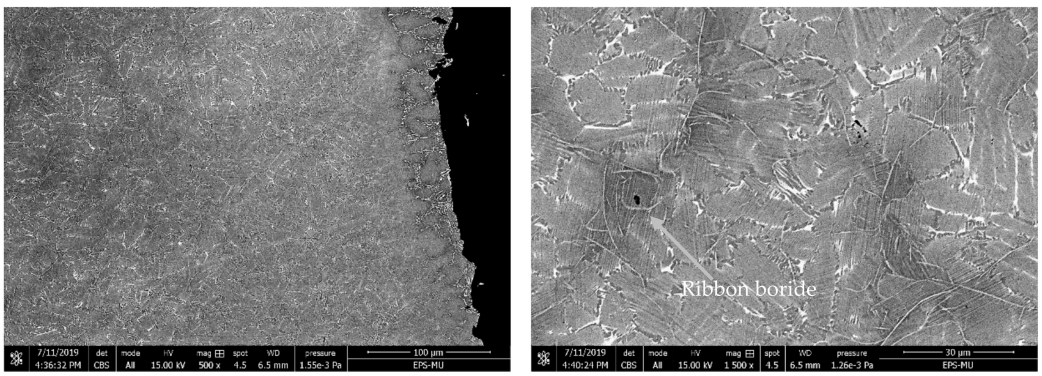

(**a**) (**b**)

Figure 6. BSE image of the 2-mm step of the modified TNM-1.5B alloy: (**a**) ribbon borides inside segregations close to the surface and (**b**) detailed image of the ribbon borides.

3.1.2. Interior of the 16 mm Step (Slow Cooling)

The TNM-0.1B alloy exhibited micro-shrinkages in the casting arising from hot spots created during solidification. An analysis revealed mostly randomly dispersed ribbon borides, and minor segregations were detected. Nevertheless, a quite homogeneous microstructure with few blocky borides was achieved (Figure 7).

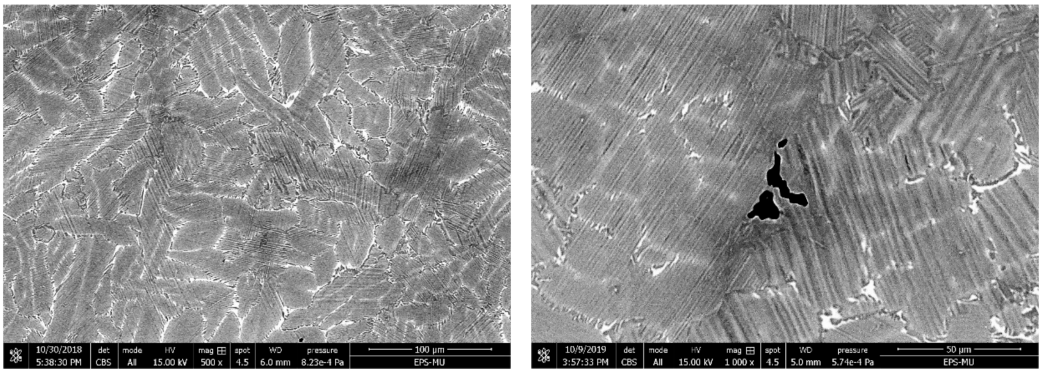

(**a**) (**b**)

Figure 7. BSE image of the 16 mm step for the TNM-0.1B alloy: (**a**) general image and (**b**) detailed image.

In the case of the modified TNM-0.6B alloy, no segregations were observed. The number of ribbon borides decreased, while the number of blocky borides increased. Consequently, the bulk alloy displayed a fine and homogeneous microstructure with a mixture of ribbon and blocky borides (Figure 8).

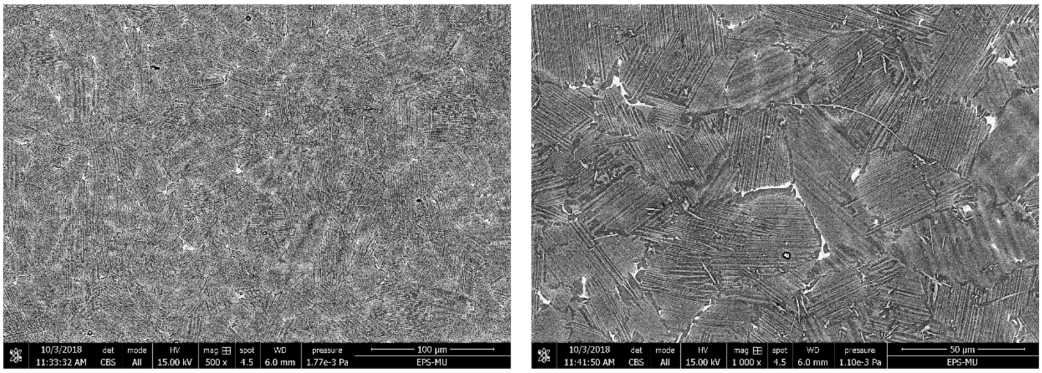

(**a**) (**b**)

Figure 8. BSE image of the 16-mm step for the modified TNM-0.6B alloy: (**a**) general image and (**b**) detailed image.

The modified TNM-1.5B alloy (Figure 9) had a similar microstructure to the modified TNM-0.6B alloy, with no segregations. However, most of the borides were of the blocky type and the ribbon borides were not typically entangled. The distribution of blocky borides was more homogeneous than in the modified TNM-0.6B alloy.

Since the modified TNM-1.5B alloy displayed the best microstructure in terms of homogeneity and fine grain, with plenty of blocky borides and no segregations, it was chosen for subsequent analysis of the effect of the cooling rate.

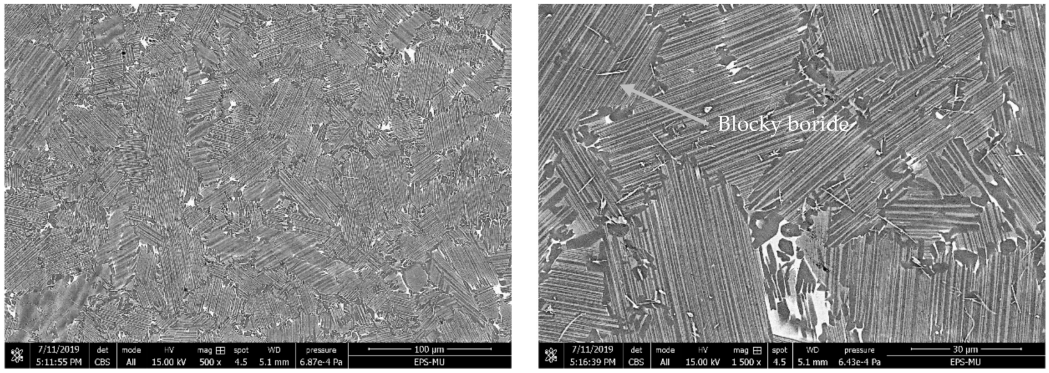

(**a**) (**b**)

Figure 9. BSE image of the 16-mm step of the modified TNM-1.5B alloy: (**a**) general image, (**b**) detailed image.

3.2. *Effect of the Cooling Rate*

To compensate for the low overheating of the ISM technology—and to achieve a more accurate solidification cooling rate—the average cooling rate during the first 5 s after pouring was calculated (Table 3). The results reveal that the 2-mm step cooled at a rate of around 50 K/s, and the 4 and 8 mm steps cooled at around 25 K/s and 5 K/s, respectively. Technical problems during the experiment prevented data acquisition for the 16-mm step, so no cooling rate was recorded. However, the computational simulation predicted a cooling rate of around 2 K/s in this sample region (Figure 10).

Table 3. Cooling rate during solidification.

Cooling Rate (K/s)	2 mm	4 mm	8 mm	* 16 mm
Experimental, first 5 s after pouring	43.8	25.6	6.8	2.3

*—Value obtained from the computational simulation.

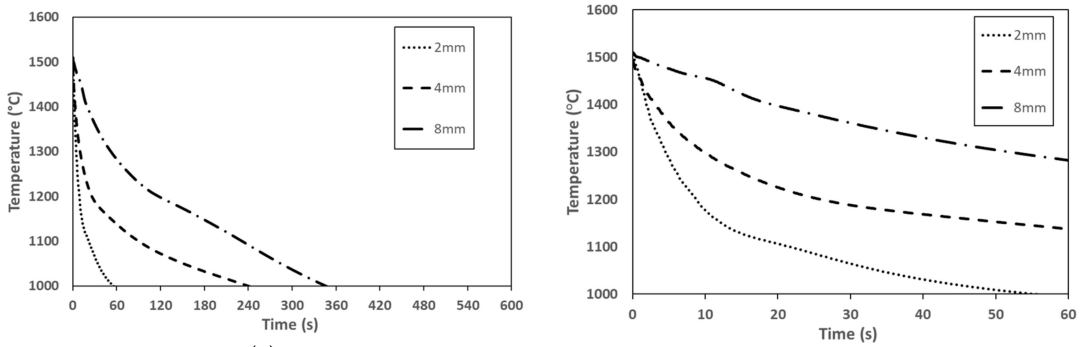

(**a**) (**b**)

Figure 10. Experimental cooling curves of the modified TNM-1.5B alloy cast in a stepped mold with 2, 4 and 8 mm thickness: (**a**) general and (**b**) detailed.

After analyzing and comparing the SEM micrographs (Figure 11) and experimentally obtained cooling curves, 10 K/s can be defined as the cooling rate limit that provides the most adequate as-cast microstructure. Above this limit, many segregations containing entangled ribbon borides were formed. Cooling rates below this limit lead to few or no segregations and the precipitation of mostly blocky borides.

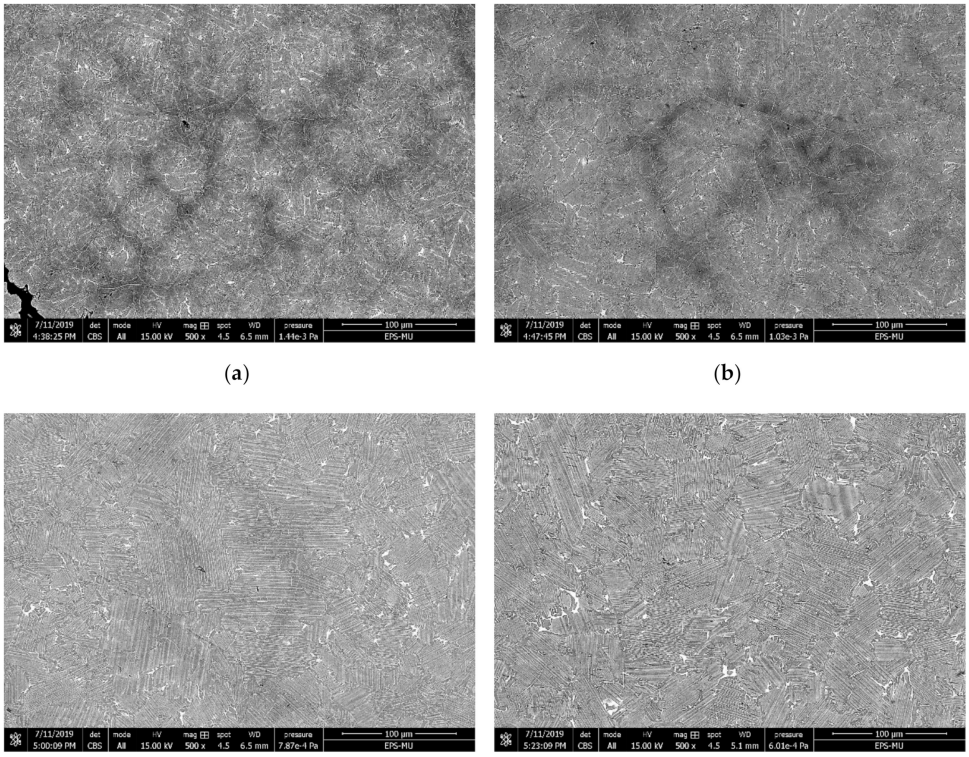

(**a**) (**b**)

(**c**) (**d**)

Figure 11. BSE image showing the general microstructure of modified TNM-1.5B alloy: (**a**) 2 mm step; (**b**) 4 mm step, (**c**) 8 mm step, (**d**) 16 mm step.

4. Discussion

The main goal of this study is to correlate the formation of blocky and ribbon borides with the chemical composition and solidification cooling rate in order to achieve a fine and homogeneous microstructure. For this purpose, the amounts of boron and aluminum were modified from the master alloy and different solidification cooling rates of the selected modified alloy were analyzed. As a result of this research, a mechanism for the formation of ribbon and blocky borides is proposed.

4.1. Effect of the Chemical Composition

Table 4 summarizes the results. On one hand, TNM alloys with boron contents below 0.5 at.% seem to promote the formation of segregations with detrimental ribbon borides, especially in areas subjected to high cooling rates during solidification. On the other hand, boron contents above 0.5 at.% help to precipitate beneficial blocky borides, particularly in areas with low solidification cooling rates.

Table 4. Summary of the effect of chemical composition on the microstructure and type of boride to be precipitated.

Alloy		TNM-0.1B	TNM-0.6B	TNM-1.5B
Location	Surface of 2 mm step (fast cooling)	Many entangled ribbon borides and segregations	Randomly dispersed ribbon borides and segregations, with some blocky borides	Randomly dispersed ribbon borides and segregations, with some blocky borides
	Inside 16 mm step (slow cooling)	Minor segregations with ribbons and few blocky borides	No segregations and mixture of ribbons and blocky borides	No segregations with many blocky and few ribbon borides

4.2. Effect of Cooling Rate

The 2 and 4 mm steps (fast cooling regions) cooled at rates above 10 K/s and they displayed segregations with ribbon borides inside. Thus, it can be concluded that these are not ideal microstructures. Cooling rates below 10 K/s led to a homogeneous and fine microstructure and therefore can be considered beneficial for the mechanical behavior of the alloy. This phenomenon seems to be related to equilibrium and disequilibrium conditions, in which the cooling rate and chemical composition are the parameters with the most influence. Therefore, for a better understanding, a boride formation mechanism is proposed.

4.3. Boride Formation Mechanism

4.3.1. Ribbon Boride Formation Mechanism

If the boron concentration is lower than the critical value (around 0.5 at.%), then borides will not form until the liquid reaches the solubility limit for boron. As a result, progressive enrichment of the liquid occurs in boron, while the β-phase is nucleated from molybdenum and niobium, leading to a melt that becomes more enriched in aluminum and boron.

The proposed ribbon boride formation mechanism follows the principle outlined by Porter et al., entitled "near no diffusion in solid, slow diffusional mixing in liquid" [15].

During solidification, the surface of the alloy is the first region to solidify, and as a result, boron and aluminum are moved towards the interior of the melt until the solubility limit of boron in the melt is reached. Once the boron is no longer soluble in the liquid due to its local high concentration and low solubility in aluminum [14], precipitation of ribbon borides in the form of chains/flakes takes place. Aluminum is enriched in these areas because of the depletion of β-stabilizing elements. Figure 12 shows the concentration profile based on the depth starting from the surface (of the mold) and the formation of ribbon borides.

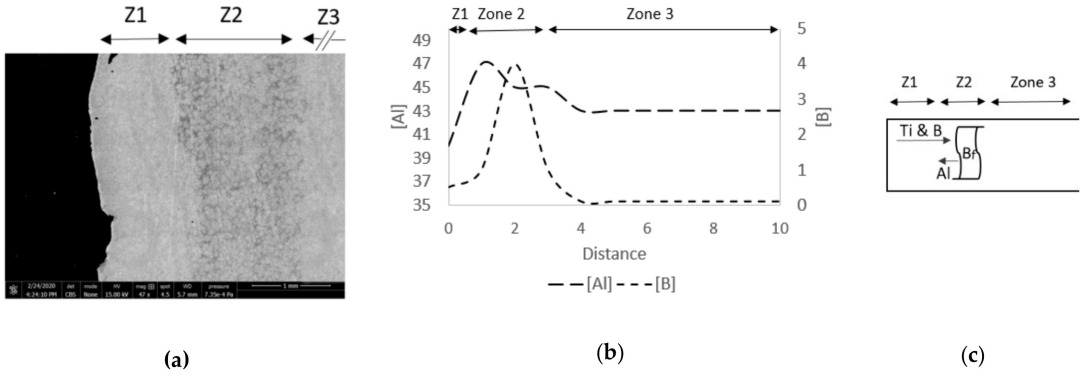

Figure 12. Ribbon boride formation mechanism: (**a**) scanning electron microscopy (SEM) micrograph, (**b**) elemental concentration profile from the surface, (**c**) 2D depiction of the formation mechanism of the ribbon boride.

Zone 1: Movement of boron and aluminum towards the interior;
Zone 2: Precipitation of ribbon borides once the solubility limit of boron and aluminum is reached;
Zone 3: Progressive restoration of the nominal chemical composition;

An overly high solidification cooling rate leads to the formation of ribbon borides, even if the boron concentration is high enough, due to the localized depletion of boron under non-equilibrium solidification conditions.

4.3.2. Blocky Boride Formation Mechanism

Blocky borides tend to appear when the boron content is higher than the critical value (around 0.5 at.%), through random precipitation before the end of solidification, especially when

the cooling rate is lower than 10 K/s. This leads to a grain refinement effect during the solid-state transformation from the β-phase to the α-phase, and hence, better mechanical properties can be achieved [10,13].

Blocky borides are formed of a mixture of titanium, boron and a little bit of niobium, but they reject aluminum (Figure 13). Due to the high melting point of niobium, it may act as a nucleant for these borides.

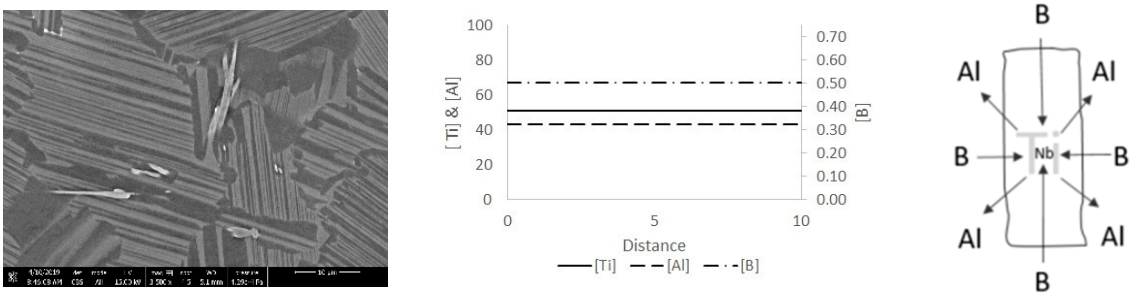

(**a**) (**b**) (**c**)

Figure 13. Stick-shaped blocky boride formation mechanism: (**a**) SEM micrograph, (**b**) elemental concentration profile from the surface, (**c**) 2D depiction of the formation mechanism of the blocky boride.

Due to homogeneity in the specimen, there was no microscopic chemical composition gradient.

It is important to highlight that even if the amount of boron is high enough to precipitate blocky borides, the cooling rate should not be too high (in the present study, a solidification cooling rate below 10 K/s is recommended) in order to prevent local disequilibrium, which could lead to the precipitation of ribbon borides.

5. Conclusions

This investigation aimed to relate the amount of boron and the solidification cooling rate to the type of boride that is precipitated. To this end, the boron content and cooling rate of alloys that generate a refined and homogeneous microstructure through the precipitation of blocky borides were determined. From this work, the following conclusions can be made:

(1) Ribbon borides are formed under non-equilibrium conditions. They are precipitated even if the amount of boron is high enough to precipitate blocky borides when the cooling rate is too high. Ribbons are formed mainly inside segregations due to their rejection of aluminum. As a result, large lamellar colonies are formed with entangled ribbon borides, which are detrimental to mechanical properties;

(2) When the boron content is above a critical value (for the modified TNM alloy, above 0.5 at.%) and the cooling rate during solidification is below 10 K/s, blocky borides are precipitated under equilibrium conditions;

(3) Boron contents above the critical value and intermediate cooling rates are associated with the precipitation of a mixture of ribbon and blocky borides. The cooling rate during solidification seems to be more relevant than chemical composition to the precipitation of either ribbon or blocky borides. Therefore, in order to obtain a refined microstructure with no segregation, a cooling rate below 10 K/s and a boron content above the critical value must be ensured.

Author Contributions: D.B. and X.C. designed and performed the experiments, D.B. and X.C. analyzed the data and wrote the study. I.H. and I.M. guided and supervised all the work carried out in this research. All authors have read and agreed to the published version of the manuscript.

Funding: This research was funded by the HAZITEK program of the RVCTI.

Acknowledgments: The authors would like to sincerely thank the Department of Education, Universities and Research of the Basque Government for its financial support by means of TALDEA project (ZE-2017/00,029).

Conflicts of Interest: The authors declare no conflict of interest.

References

1. Appel, F.; Paul, J.; Oehring, M. *Gamma Titanium Aluminide Alloys*; Wiley: Weinheim, Germany, 2014.
2. Kim, Y.W.; Kim, S.L. Advances in gammalloy materials-processes-application technology: Successes, dilemmas, and future. *JOM* **2018**, *70*, 553–560. [CrossRef]
3. Habel, U.; Heutling, F.; Kunze, C.; Smarsly, W.; Das, G.; Clemens, H. Forged intermetallic γ-TiAl based alloy low pressure turbine blade in the geared turbofan. In Proceedings of the 13th World Conference on Titanium, San Diego, CA, USA, 16–20 August 2016; pp. 1223–1227.
4. Clemens, H.; Wallgram, W.; Kremmer, S.; Güther, V.; Otto, A.; Bartels, A. Design of novel β-solidifying TiAl alloys with adjustable β/B2-phase fraction and excellent hot-workability. *Adv. Eng. Mater.* **2008**, *10*, 707–713. [CrossRef]
5. Hecht, U.; Witusiewicz, V.; Drevermann, A.; Zollinger, J. Grain refinement by low boron additions in niobium-rich TiAl-based alloys. *Intermetallics* **2008**, *16*, 969–978. [CrossRef]
6. Kastenhuber, M.; Klein, T.; Rashkova, B.; Weißensteiner, I.; Clemens, H.; Mayer, S. Phase transformations in a β-solidifying γ-TiAl based alloy during rapid solidification. *Intermetallics* **2017**, *91*, 100–109. [CrossRef]
7. Cheng, T.T. Mechanism of grain refinement in TiAl alloys by boron addition-An alternative hypothesis. *Intermetallics* **2000**, *8*, 29–37. [CrossRef]
8. Yang, C.; Jiang, H.; Hu, D.; Huang, A.; Dixon, M. Effect of boron concentration on phase transformation texture in as-solidified Ti44Al8Nb x B. *Scr. Mater.* **2012**, *67*, 85–88. [CrossRef]
9. Kitkamthorn, U.; Zhang, L.C.; Aindow, M. The structure of ribbon borides in a Ti-44Al-4Nb-4Zr-1B alloy. *Intermetallics* **2006**, *14*, 759–769. [CrossRef]
10. Hu, D. Role of boron in TiAl alloy development: A review. *Rare Met.* **2016**, *35*, 1–14. [CrossRef]
11. Klein, T.; Clemens, H.; Mayer, S. Advancement of compositional and microstructural design of intermetallic γ-TiAl based alloys determined by atom probe tomography. *Materials* **2016**, *9*, 755. [CrossRef] [PubMed]
12. Kartavykh, A.V.; Gorshenkov, M.V.; Podgorny, D.A. Grain re fi nement mechanism in advanced γ-TiAl boron-alloyed structural intermetallics: The direct observation. *Mater. Lett.* **2015**, *142*, 294–298. [CrossRef]
13. Oehring, M.; Stark, A.; Paul, J.D.H.; Lippmann, T.; Pyczak, F. Microstructural refinement of boron-containing β-solidifying γ-titanium aluminide alloys through heat treatments in the β phase field. *Intermetallics* **2013**, *32*, 12–20. [CrossRef]
14. Witusiewicz, V.T.; Bondar, A.A.; Hecht, U.; Zollinger, J.; Artyukh, L.V.; Velikanova, T.Y. The Al-B-Nb-Ti system. V. Thermodynamic description of the ternary system Al-B-Ti. *J. Alloy. Compd.* **2009**, *474*, 86–104. [CrossRef]
15. Porter, D.A.; Easterling, K.E. *Phase Transformations in Metals and Alloys*; Springer-Science + Business Media, B.V.: Hong Kong, China, 1992.